ELSEVIER

Cardiovascular Research 66 (2005) 520–529

Cardiovascular Research

www.elsevier.com/locate/cardiores

Blockade of NF-κB improves cardiac function and survival without affecting inflammation in TNF-α-induced cardiomyopathy

Natsumi Kawamura[a], Toru Kubota[a,*], Shunichi Kawano[a], Yoshiya Monden[a], Arthur M. Feldman[b], Hiroyuki Tsutsui[a], Akira Takeshita[a], Kenji Sunagawa[a]

[a]*Department of Cardiovascular Medicine, Kyushu University Graduate School of Medical Sciences, 3-1-1 Maidashi, Higashi-ku, Fukuoka 812-8582, Japan*
[b]*Department of Medicine, Jefferson Medical College, Philadelphia, PA, USA*

Received 18 October 2004; received in revised form 7 February 2005; accepted 7 February 2005
Available online 8 March 2005
Time for primary review 23 days

Abstract

Objective: NF-κB, a key transcription factor that regulates inflammatory processes, has been shown to be activated in the failing human heart with enhanced expression of proinflammatory cytokines. In the present study, we assessed the hypothesis that cardiotoxic effects of proinflammatory cytokines are mediated by the activation of NF-κB.
Methods: Transgenic mice with cardiac-specific overexpression of TNF-α were used as a model of cytokine-induced cardiomyopathy. To block the activation of NF-κB, transgenic mice (TG/p50$^{+/+}$) were crossed with knockout mice in which the p50 subunit of NF-κB was disrupted (WT/p50$^{-/-}$).
Results: The electrophoretic mobility shift assay demonstrated that NF-κB was activated in the myocardium of TG/p50$^{+/+}$ mice, while it was completely abolished in TG/p50$^{-/-}$ mice. Male TG mice died of congestive heart failure earlier than females, where the disruption of the p50 subunit significantly improved the survival. Compared with TG/p50$^{+/+}$ mice, TG/p50$^{-/-}$ mice showed a significant reduction of ventricular dilatation and hypertrophy with preserved fractional shortening. Although the myocardial expression of proinflammatory cytokines or infiltration of inflammatory cells was not affected, increased expression and activity of MMP-9 were significantly suppressed in TG/p50$^{-/-}$ mice.
Conclusion: Blockade of NF-κB activation did not ameliorate myocardial inflammation but improved cardiac function and survival in male TNF-α TG mice. An inhibition of NF-κB may be a new therapeutic strategy for cardiac remodeling and heart failure, especially when proinflammatory cytokines are activated.

Keywords: Nuclear factor-κB; Cytokines; Tumor necrosis factor-α; Matrix metalloproteinases; Transgenic animal models; Myocarditis; Heart failure; Cardiac remodeling

1. Introduction

Tumor necrosis factor (TNF)-α is a proinflammatory cytokine, which exerts a wide range of biological activities [1]. TNF-α may play an important role in the pathogenesis of congestive heart failure for the following reasons. First, plasma levels of TNF-α are elevated in patients with congestive heart failure [2,3]. Second, the failing human heart expresses a substantial amount of TNF-α [4,5]. Third, studies in vitro have shown that TNF-α suppresses cardiac contractility [6,7], provokes myocardial hypertrophy [8,9], and induces apoptosis in cardiac myocytes [10]. To investigate the pathophysiological significance of myocardial production of TNF-α in vivo, we have made transgenic mice that overexpress TNF-α specifically in the heart under the control of α-myosin heavy chain promoter [11]. These mice present myocardial inflammation, ventricular dilatation, and con-

* Corresponding author. Tel.: +81 92 642 5360; fax: +81 92 642 5374.
E-mail address: kubotat@cardiol.med.kyushu-u.ac.jp (T. Kubota).

0008-6363/$ - see front matter © 2005 European Society of Cardiology. Published by Elsevier B.V. All rights reserved.
doi:10.1016/j.cardiores.2005.02.007

gestive heart failure. Furthermore, male mice die younger than females [12,13]. Treatment with soluble TNF receptors reverse myocardial inflammation, extracellular matrix remodeling, and ventricular dysfunction in these mice [14,15]. Several aspects of these results have since been confirmed by another laboratory [16]. Thus, myocardial production of TNF-α may play an important role in the development of congestive heart failure. However, the mechanisms by which TNF-α damages the myocardium remain undetermined.

Nuclear factor-kappa B (NF-κB) is a key transcription factor that regulates inflammatory processes [17]. Many stimuli activate NF-κB, including proinflammatory cytokines, lipopolysaccharide, and reactive oxygen species. Activation of NF-κB involves the phosphorylation and subsequent proteolytic degradation of the inhibitory protein IκB by specific IκB kinases. The free NF-κB (typically, a heterodimer of p50 and p65) then passes into the nucleus, where it binds to κB sites in the promoter regions of genes for inflammatory proteins such as TNF-α, inducible nitric oxide synthase, and adhesion molecules. Thus the activation of NF-κB leads to a coordinated increase in the expression of many genes whose products mediate inflammatory and immune responses [17]. Furthermore, the activation of NF-κB may also play an important role in the pathogenesis of cardiac remodeling and heart failure [18], since recent in vitro studies have demonstrated that activation of NF-κB is required for hypertrophic growth of primary rat neonatal ventricular cardiomyocytes in response to angiotensin II, phenylephrine, and endothelin-1 [19,20]. Therefore, blockade of NF-κB may be a new therapeutic strategy for heart failure by attenuating myocardial inflammation and hypertrophy.

Based on these backgrounds, the present study was designed to assess the hypothesis that cardiotoxic effects of proinflammatory cytokines are mediated by the activation of NF-κB. To block the activation of NF-κB, transgenic mice with cardiac-specific overexpression of TNF-α [11] were crossed with knockout mice in which the p50 subunit of NF-κB was disrupted (WT/$p50^{-/-}$) [21]. Although the blockade of NF-κB did not ameliorate myocardial inflammation, it significantly improved cardiac function and survival in male TNF-α transgenic mice. These results support the hypothesis that the activation of NF-κB may play an important role in myocardial dysfunction and remodeling besides promoting inflammation.

2. Methods

2.1. Animal model

Transgenic mice with cardiac-specific overexpression of TNF-α (TNF TG) [11] and wild-type littermates (WT) were studied. To block the activation of NF-κB, TNF TG mice were crossed with knockout mice in which the p50 subunit of NF-κB was disrupted ($p50^{-/-}$ KO) [21]. Since the genetic background of TNF TG mice (FVB) was different from that of $p50^{-/-}$ KO mice (B6, 129), $p50^{-/-}$ KO mice were first backcrossed onto the FVB strain for five generations. Then, $p50^{+/-}$ KO males (F5) were mated with TNF TG females to yield WT or TG mice with $p50^{+/+}$ or $p50^{+/-}$ (F6). Subsequently, TG/$p50^{+/-}$ females were mated with WT/$p50^{+/-}$ males to obtain TG or WT mice with $p50^{+/+}$, $p50^{+/-}$, or $p50^{-/-}$ (F7), which were studied in the present study. Littermates were studied in each analysis to assure the minimization of genetic background variation. All the mice studied were males unless mentioned otherwise. This study was reviewed by the Committee of the Ethics on Animal Experiment, Kyushu University Graduate School of Medical Sciences and carried out under the control of the Guideline for Animal Experiment, Kyushu University and the Law (No. 105) and Notification (No. 6) of the Government. The investigation conforms to the Guide for the Care and Use of Laboratory Animals published by the US National Institutes of Health (NIH Publication No. 85-23, revised 1996).

2.2. Electrophoretic mobility shift assay

Electrophoretic mobility shift assays (EMSA) were performed according to the manufacturer's instructions (Gel Shift Assay System E3300, Promega, Madison, Wisconsin, USA) as previously described [22]. Nuclear proteins were isolated using the method of Haudek [23]. Protein concentrations were measured by BCA Protein Assay Reagents (PIERCE, Rockford, Illinois, USA) using bovine serum albumin (BSA) as a standard. Protein-DNA binding was carried out in a final volume of 40 μl. To each tube, 4 μl of 10×binding buffer (100 mmol/l Tris pH 8.0, 10 mmol/l EDTA, 40% glycerol, 1 mol/l NaCl), 100 ng of 1,4-dithiothreitol (DTT), 4 μg of BSA, 2 μg of dIdC, and 30 μg nuclear proteins were added. After the samples were incubated at room temperature for 10 min, 1 μl of ^{32}P-labeled NF-κB probe (a double-stranded oligonucleotide corresponding to the consensus NF-κB binding site of the κ light-chain enhancer: 5′-AGTTGAGGGGACTTTCCCAGGC-3′, approximately 20000 cpm/ng) was added to each reaction and incubate for 20 min at room temperature. For supershift reactions, 1 μl of anti-p50 or p65 antibody (sc-114X or sc-472X: Santa Cruz, Paso Robles, California, USA) was added after 20 min binding reaction with further incubation of 30 min on ice. Samples were resolved on a 5% acrylamide gel in 0.25% TBE buffer.

2.3. Echocardiography

Echocardiographic studies were performed using an ultrasonographic system (ALOKA SSD-5500; Tokyo, Japan) as previously described [13]. Under anesthesia

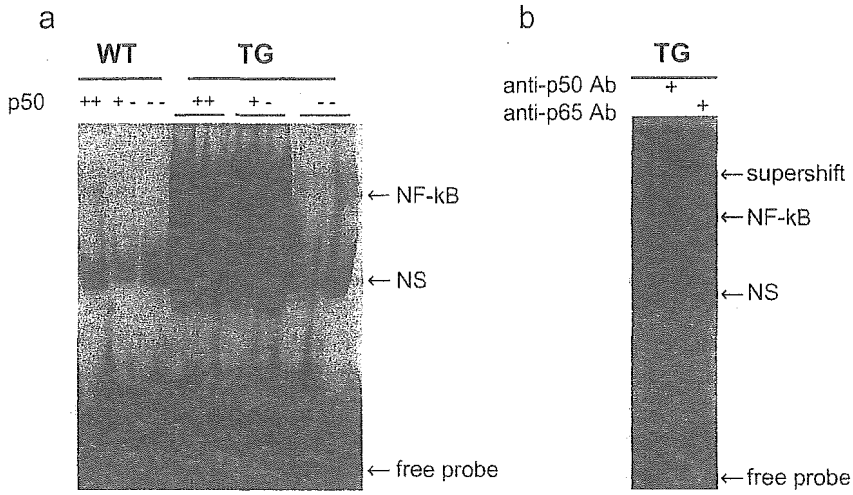

Fig. 1. Electrophoretic mobility shift assay for myocardial NF-κB activation. Nuclear proteins were isolated from wild-type (WT) or TNF-α transgenic mice (TG) with or without p50 gene (a). Super-shift analysis was performed with anti-p50 or p65 antibody to investigate the composition of activated NF-κB in TG/$p50^{+/+}$ mice (b).

with 2.5% Avertin (14 μl/g body weight, IP, Aldrich Chemical), mice were placed in a supine position. A 10-MHz transducer (ALOKA) was applied to the left hemithorax. Two-dimensional targeted M-mode imaging was obtained from the short axis view at the level of the greatest LV dimension. M-mode measurements of LV end-diastolic diameter (EDD), LV end-systolic diameter (ESD), and LV anterior and posterior wall thicknesses were made using the leading edge convention of the American Society of Echocardiography. End diastole was determined at the maximal LV diastolic dimension, and end systole was taken at the peak of posterior wall motion. The percentage of LV fractional shortening (FS) was calculated as follows: FS (%)=(EDD−ESD)/EDD× 100 [13].

2.4. Pathological analysis

After measurement of body and heart weight, tissues were fixed in 10% neutral buffered formalin for hematoxylin and eosin staining or snap-frozen in liquid nitrogen for RNA and protein analysis. Cross-sectional area of cardiomyocytes in the left ventricle was evaluated as previously reported [24]. Myocardial infiltration was quantified by determination of nuclear density (nuclei/mm^2) [14]. Our previous study using immunohistochemical analysis has demonstrated that most of the infiltrating cells in TNF TG mice are macrophages and CD-4-positive lymphocytes [25]. Because it is difficult to differentiate inflammatory cells from myocytes and/or fibroblasts, by simple hematoxylin and eosin staining, all nuclei were included in the present

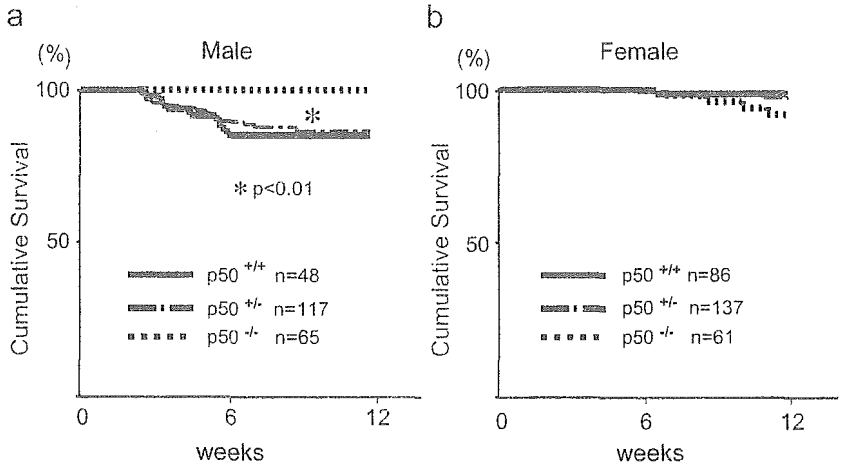

Fig. 2. Kaplan–Meier survival curves of TNF-α transgenic mice: males (a) or females (b) with or without p50 gene ($p50^{+/+}$, $p50^{+/-}$, $p50^{-/-}$). *$p<0.01$ vs. TG/$p50^{+/+}$ mice.

study. In each mice, five independent high-power fields were analyzed and averaged.

2.5. RNase protection assay

Total RNA was extracted from the left ventricle by an acid guanidium thiocyanate–phenolchloroform method. Multi-probe RNase protection assays (RPA) were performed according to the manufacturer's protocol (RiboQuant, PharMingen, San Diego, California, USA) using mMMP-1 (No. 551276), and a custom template set containing probes for murine RANTES, TNF-α, IL-6, IL-1β, TGF-β, monocyte chemotactic protein-1 (MCP-1), L32, and GAPDH (No. 557310) [14]. The value of each hybridized probe was normalized to that of GAPDH included in each template set as an internal control.

2.6. MMP zymography

Gelatin zymography was performed as previously described [26]. The myocardial samples were homogenized (~30-s bursts) in 1 ml of an ice-cold extraction buffer containing cacodylic acid (10 mmol/l), NaCl (0.15 mol/l), $ZnCl_2$ (20 mmol/l), NaN_2 (1.5 mmol/l), and 0.01% Triton X-100 (pH 5.0). The homogenate was then centrifuged (4 °C, 10 min, 10,000×g), and the supernatant was decanted and saved on ice. The pH levels of the samples were adjusted to 7.5 using Tris (1 mol/l). The final protein concentration of the myocardial extract was determined using a standardized colorimetric assay. The extracted samples were then aliquoted and stored at −80 °C until the time of assay. The myocardial extracts were then directly loaded onto electrophoretic gels (SDS-PAGE) containing 1 mg/ml gelatin under nonreducing conditions. The myocardial extracts at a final protein content of 5 μg were loaded onto the gels using a 3:1 sample buffer (10% SDS, 4% sucrose, 0.25 mol/l Tris–HCl, and 0.1% bromophenol blue; pH 6.8). The gels were run at 15 mA/gel through the stacking phase (4%) and at 20 mA/gel for the separating phase (10%) while the running buffer temperature was maintained at 4 °C. After SDS-PAGE, the gels were washed twice in 2.5% Triton X-100 for 30 min each, rinsed in water, and incubated for 24 h in a substrate buffer at 37 °C (50 mmol/l Tris–HCl, 5 mmol/l $CaCl_2$, and 0.02% NaN_3; pH 7.5). After incubation, the gels were stained with Coomassie brilliant blue R-250. The zymograms were digitized, and the size-fractionated bands, which indicated the MMP proteolytic levels, were measured by the integrated optical density in a rectangular region of interest.

2.7. Statistical analysis

The results are presented as mean±S.D. Statistical comparisons were performed using ANOVA with Student's–Newman–Keuls post-hoc test or unmatched Student's t-test where appropriate. Survival analysis was performed by the Kaplan–Meier method, and between-group difference in survival was tested by the log-rank test. Differences were considered significant at a value of $P<0.05$.

3. Results

3.1. NF-κB KO abolishes activation of NF-κB in TNF TG myocardium

NF-κB was activated in the myocardium of TNF TG/p50ce$^{+/+}$ mice, while it was completely abolished in TNF TG/p50$^{-/-}$ mice (Fig. 1a). Since most of NF-κB band was

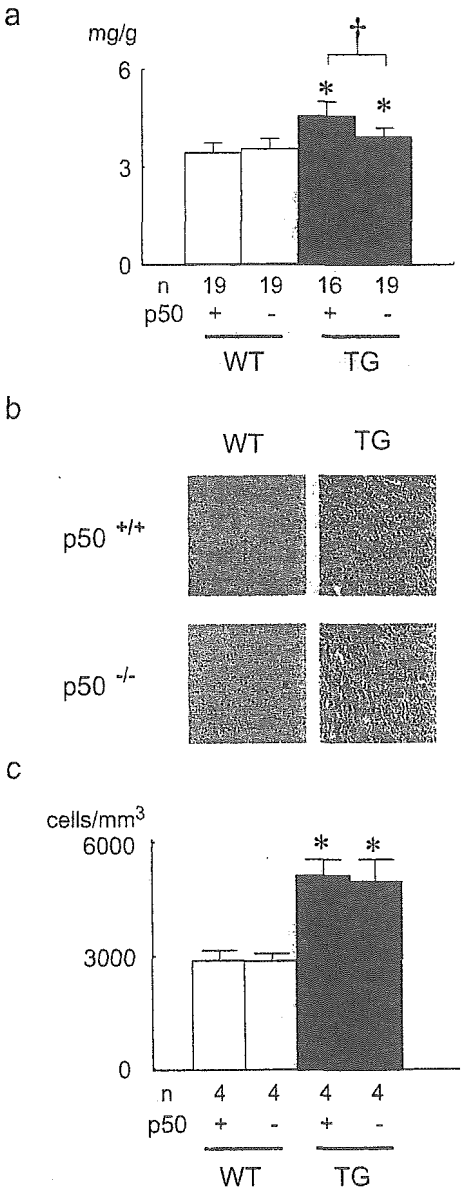

Fig. 3. Pathological analysis of the heart: left ventricular weight (a), hematoxylin–eosin staining (b), and cell density (c). Values are mean±S.D. WT indicates wild-type mice; TG, TNF-α transgenic mice. *$p<0.05$ vs. WT/p50$^{+/+}$ mice, †$P<0.05$ vs. TG/p50$^{+/+}$ mice.

super-shifted with the anti-p50 antibody but not with the anti-p65 antibody, the majority of NF-κB was suggested to be p50–p50 homodimers in TNF TG/p50$^{+/+}$ mice (Fig. 1b).

3.2. NF-κB KO improves the survival of TNF TG males

Consistent with previous studies [12,13], mortality was significantly lower in female TNF TG/p50$^{+/+}$ mice when compared with male TNF TG/p50$^{+/+}$ mice (P<0.005, Fig. 2). Thus, NF-κB KO did not affect the survival of TNF TG females as only one of 86 TG/p50$^{+/+}$, three of 137 TG/p50$^{+/-}$, and four of 61 TG/p50$^{-/-}$ died by the end of 12 weeks (P=0.108). In contrast, NF-κB KO significantly improved the survival of TNF TG males (P<0.01) as seven of 48 TG/p50$^{+/+}$ and 15 of 117 TG/p50$^{+/-}$, but none of 65 TG/p50$^{-/-}$, died by the end of 12 weeks. All the mice that died spontaneously exhibited exceptional dilatation of the heart and pleural effusion, suggesting that they died of congestive heart failure [11]. To elucidate the mechanisms by which NF-κB improves the survival of TNF TG mice, the following studies were focused on TNF TG males KO with p50$^{+/+}$ or p50$^{-/-}$ at the age of 6 weeks.

3.3. NF-κB KO suppresses cardiac hypertrophy without ameliorating myocardial inflammation

As shown in Fig. 3a, the left ventricle of TG mice weighted significantly more than that of WT mice as previously reported [11]. NF-κB KO significantly attenuated ventricular hypertrophy in TNF TG males. After hematoxylin–eosin staining, cross-sectional area of cardiomyocytes was evaluated: WT/p50$^{+/+}$ (n=3), 234±24 (S.D.) μm^2; WT/p50$^{-/-}$ (2), 245±50; TNF TG/p50$^{+/+}$ (5), 260±70; TNF TG/p50$^{-/-}$ (5), 195±29 (p=0.27). Despite the attenuation of ventricular hypertrophy by NF-κB KO, differences in cross-sectional were not statistically significant among the four groups. Since we have previously reported that the cardiomyocyte hypertrophy in TNF TG mice was primarily attributable to the elongation of the resting cell length without widening of the cell width [27], the attenuation of ventricular hypertrophy by NF-κB KO may be attributable to suppression of cardiomyocyte elongation in TNF TG mice. As shown in Fig. 3b, a marked infiltration of inflammatory cells was observed in the myocardium of TNF TG mice. The number of cells in the myocardium was significantly increased in TNF TG mice, although it was not affected by NF-κB KO (Fig. 3c). No significant difference was observed between TG/p50$^{+/+}$ and TG/p50$^{-/-}$ mice.

To further assess the severity of myocardial inflammation, expression of proinflammatory cytokines was evaluated by multi-probe RPA (Fig. 4). Transcript levels of IL-1β, TGF-β, MCP-1, and RANTES as well as TNF-α were significantly increased in TNF TG myocardium. Since no significant differences were observed between TG/p50$^{+/+}$ and TG/p50$^{-/-}$ mice, NF-κB KO did not attenuate myocardial expression of proinflammatory cytokines. These results indicate that NF-κB KO ameliorates myocardial hypertrophy without affecting myocardial inflammation in TNF TG mice.

3.4. NF-κB KO reverses cardiac dysfunction and remodeling

Echocardiography was performed to evaluate cardiac function and remodeling in these mice (Fig. 5a). TNF TG/p50$^{+/+}$ mice exhibited ventricular dilatation with reduced fractional shortening. As summarized in Fig. 5b and Table 1, NF-κB KO significantly ameliorated ventricular dilatation and improved the fractional shortening in TNF TG

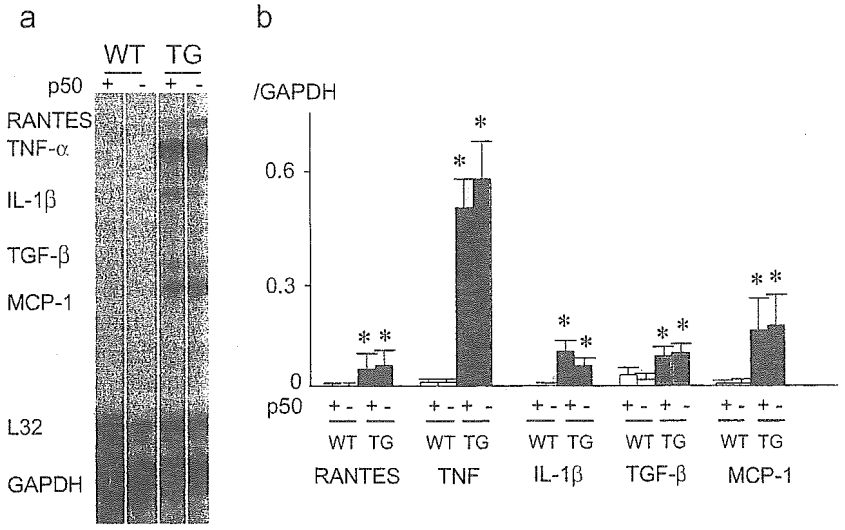

Fig. 4. Multi-probe RNase protection assay for cytokines in myocardium: representative images (a) and summarized data (b). Values are mean±S.D. WT indicates wild-type mice; TG, TNF-α transgenic mice. *P<0.05 vs. WT/p50$^{+/+}$ mice.

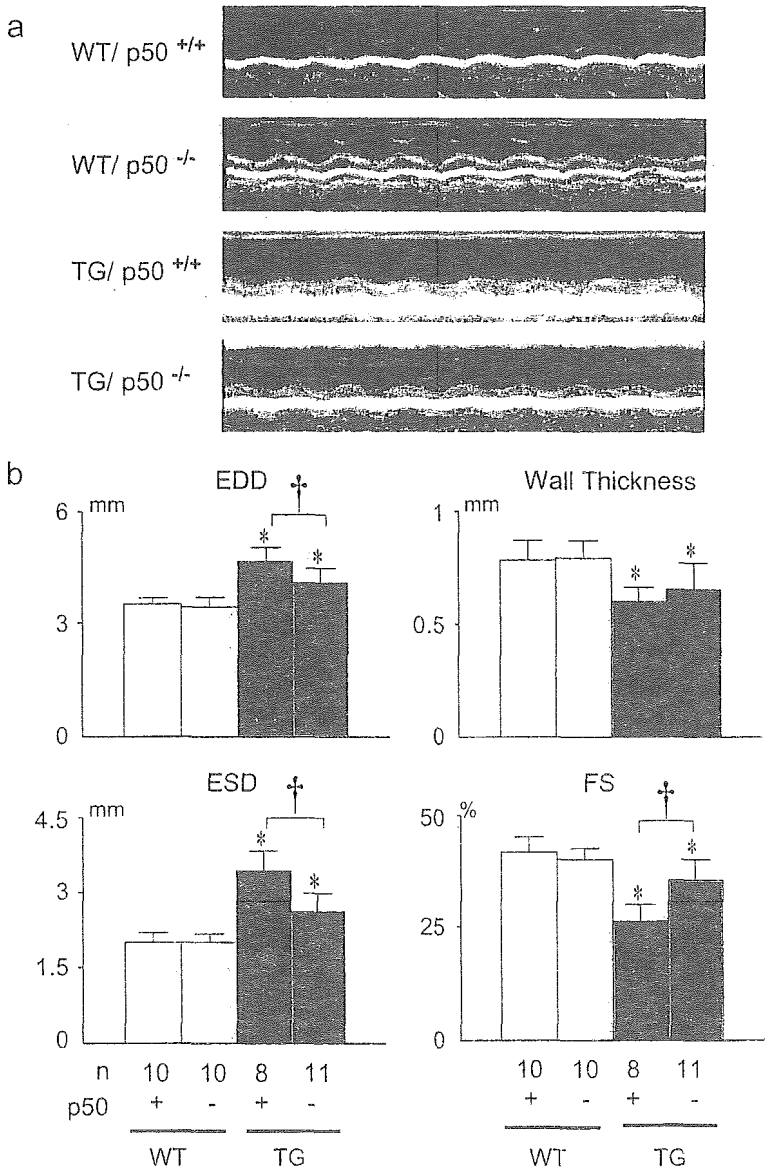

Fig. 5. Echocardiographic analysis of ventricular structure and function: representative images of M-mode echocardiogram (a) and summarized data (b). Values are mean±S.D. WT indicates wild-type mice; TG, TNF-α transgenic mice; EDD, end-diastolic diameter; ESD, end-systolic diameter; FS, fractional shortening. *$p<0.05$ vs. WT/p50$^{+/+}$ mice, †$P<0.05$ vs. TG/p50$^{+/+}$ mice.

mice. These results suggest that, despite persistent expression of proinflammatory cytokines in the myocardium, NF-κB KO improves cardiac function and restrains ventricular remodeling in TNF TG mice.

3.5. NF-κB KO blocks MMP-9 activation

Transcript levels of MMPs and TIMPs were evaluated by multi-probe RPA (Fig. 6a). MMP-2, MMP-9, and TIMP-1 were increased, while TIMP-4 was decreased, in TNF TG/p50$^{+/+}$ myocardium. As summarized in Fig. 6b, NF-κB KO significantly suppressed the up-regulation of MMP-9 in TNF TG mice, although it did not affect that of MMP-2 or TIMP1, or the down-regulation of TIMP-4. To take into account of the interactions between MMPs and TIMPs in these mice, the ratios of MMP-2/TIMP-2 and MMP-9/TIMP-1 were summarized in Table 2. Although there was a trend of higher MMP-2/TIMP-2 in TNF TG mice, the up-regulation of MMP-2 was not statistically significant after normalization with TIMP-2. In contrast, although both MMP-9 and TIMP-1 were up-regulated in TNF TG mice, the ratio of MMP-9/TIMP-1 was still significantly higher in TNF TG mice. As in the case of MMP-9, NF-κB KO significantly abrogated the up-regulation of MMP-9/TIMP-1 ratio in TNF TG mice. To further confirm the specific abrogation of MMP-9 activity in TNF TG/p50$^{-/-}$ mice, zymography was performed as shown in Fig. 7. Although a slight but significant increase of MMP-2 activity in TNF TG mice was not affected, the marked increase of MMP-9 activity

Table 1
Echocardiographic parameters

	WT/p50$^{+/+}$	WT/p50$^{-/-}$	TNF TG/p50$^{+/+}$	TNF TG/p50$^{-/-}$
n	10	10	8	11
EDD (mm)	3.49±0.15	3.42±0.23	4.64±0.37*	4.06±0.40*,†
ESD (mm)	2.01±0.19	2.01±0.14	3.44±0.37*	2.61±0.36*,†
FS (%)	41.7±3.3	40.0±2.6	26.4±3.7*	35.6±4.5*,†
Wall thickness (mm)	0.78±0.09	0.79±0.07	0.60±0.06*	0.65±0.11*

Values are mean±S.D. WT indicates wild-type mice; TG, TNF-α transgenic mice; EDD, end-diastolic diameter; ESD, end-systolic diameter; FS, fractional shortening.
* $p<0.05$ vs. WT/p50$^{+/+}$ mice.
† $P<0.05$ vs. TG/p50$^{+/+}$ mice.

Table 2
Ratios of MMPs to TIMPs

	WT/p50$^{+/+}$	WT/p50$^{-/-}$	TNF TG/p50$^{+/+}$	TNF TG/p50$^{-/-}$
n	4	4	5	5
MMP-2/ TIMP-2	0.97±0.57	1.13±1.04	1.94±1.45	1.62±0.63
MMP-9/ TIMP-1	0.64±0.41	0.81±0.73	3.54±0.78*	0.59±0.30

Values are mean±S.D.
* $p<0.05$ vs. WT/p50$^{+/+}$ mice.

was significantly attenuated by NF-κB KO. Since we have previously reported that treatment with an MMP inhibitor significantly prolongs the survival of TNF TG mice [28], the selective inhibition of MMP-9 activation may contribute to cardioprotective effects of NF-κB KO on these mice.

4. Discussion

In the present study, we tested the hypothesis that cardiotoxic effects of proinflammatory cytokines are mediated by the activation of NF-κB. Transgenic mice with cardiac-specific overexpression of TNF-α [11] were used as a model of cytokine-induced cardiomyopathy and knockout mice deficient in the p50 subunit of NF-κB [21] were used to block the activation of NF-κB. The results indicated that cardiac-specific overexpression of TNF-α provoked heart failure with NF-κB activation, myocardial inflammation, ventricular hypertrophy, cardiac dysfunction, and MMP activation. Although blockade of NF-κB did not affect myocardial inflammation, it significantly reversed ventricular hypertrophy, improved cardiac function, reduced MMP-9 activity, and improved the survival of TNF-α transgenic mice. Activation of NF-κB therefore may play an important role in the pathogenesis of myocardial dysfunction and remodeling besides promoting myocardial inflammation.

Since activation of NF-κB induces various members of proinflammatory cytokines and chemokines [17], and blockade of NF-κB activation has been shown to reduce inflammatory response and damage after cardiac ischemia and reperfusion [29], we had hypothesized that the blockade of NF-κB might attenuate myocardial inflammation observed in TNF TG mice. However, the results did not

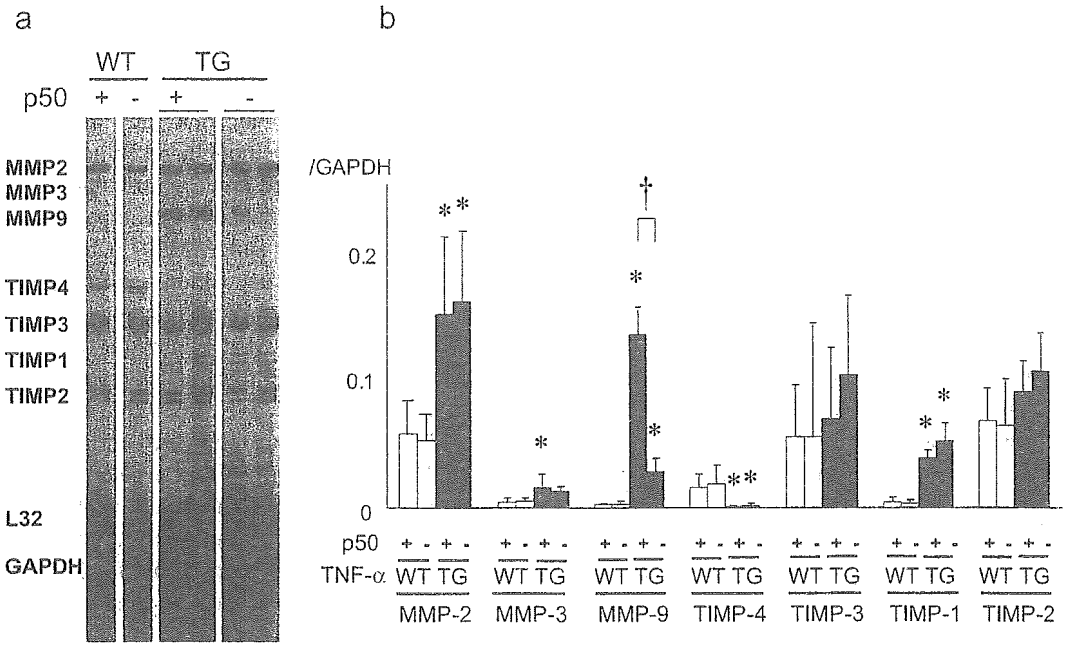

Fig. 6. Multi-probe RNase protection assay for MMPs and TIMPs in myocardium: representative images (a) and summarized data (b). Values are mean±S.D. WT indicates wild-type mice; TG, TNF-α transgenic mice. *$p<0.05$ vs. WT/p50$^{+/+}$ mice, †$P<0.05$ vs. TG/p50$^{+/+}$ mice.

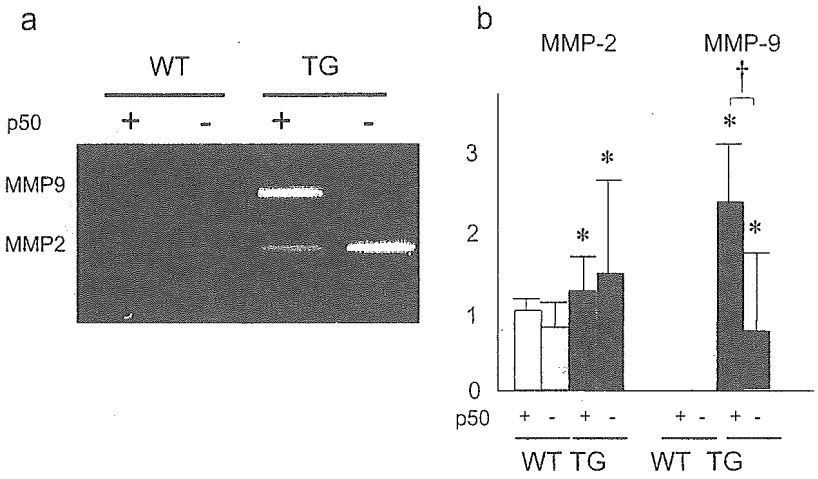

Fig. 7. Gelatin zymography for MMP-2 and MMP-9 in myocardium: representative images (a) and summarized data (b). Values are mean±S.D. (n=4 each). WT indicates wild-type mice; TG, TNF-α transgenic mice. *p<0.05 vs. WT/p50$^{+/+}$ mice, †P<0.05 vs. TG/p50$^{+/+}$ mice.

support our hypothesis: the blockade of NF-κB activation did not affect myocardial expression of proinflammatory cytokines or chemokines, or infiltration of inflammatory cells in TG myocardium. Since we have previously reported that blockade of TNF-α abrogates myocardial inflammation of TNF TG mice [14], induction of proinflammatory cytokines and chemokines and infiltration of inflammatory cells observed in TNF TG mice are provoked by TNF-α-dependent but NF-κB-independent pathways, including ceramide, ERK, phospholipase A2, and JNK [1].

The NF-κB/Rel family consists of five subunit members, including p50, p52, c-Rel, RelA (p65), and RelB [17]. In most cells, NF-κB is a heterodimer of p50 and p65 that is retained in the cytoplasm bound to the inhibitory protein IκB. Activation of NF-κB will occur when the specific IκB kinases phosphorylate the IκB. After chronic exposure to proinflammatory cytokines, including TNF-α, NF-κB has been shown to be converted from transcriptionally active p50–p65 heterodimers to transcriptionally inactive p50–p50 homodimers, which may act as a native negative feedback mechanism to prevent excessive inflammatory responses [23,30]. Since most of NF-κB band was super-shifted with the anti-p50 antibody but not with the anti-p65 antibody, the majority of NF-κB was suggested to be transcriptionally inactive p50–p50 homodimers in our TNF TG/p50$^{+/+}$ mice. This might explain why the targeted disruption of the p50 subunit did not affect myocardial expression of proinflammatory cytokines in this mouse model of cytokine-induced cardiomyopathy. NF-κB-independent pathways appear to be more important in the development of myocardial inflammation with persistent overexpression of TNF-α.

Although the blockade of NF-κB did not affect myocardial inflammation, it significantly inhibited ventricular hypertrophy and dilatation, and improved the survival of TNF TG mice. Recent in vitro studies [19,20] have demonstrated that the activation of NF-κB is required for hypertrophic growth of primary rat neonatal ventricular cardiomyocytes in response to G-protein-coupled receptor agonists, including phenylephrine, endothelin-1, and angiotensin II. The results of the present study suggest that the activation of NF-κB may also play an important role in the development of hypertrophy in response to TNF-α. Although the precise mechanisms by which NF-κB mediates cardiac hypertrophy remain undetermined, it is of interest that the p50 subunit of NF-κB interacts with the transcription factor Krüppel-like factor 5 [31], an essential regulator of cardiovascular remodeling as manifested by a hypertrophic response to angiotensin II [32]. Therefore, the p50 is not only a subunit of NF-κB but may also interact with other transcription factors to exert versatile effects on cardiac hypertrophy and remodeling.

Matrix metalloproteinases (MMPs) are a family of proteolytic enzymes that degrade the extracellular matrix components [33]. MMPs are increased in the failing human heart, and may play an important role in the process of cardiac remodeling [34]. We have previously reported that progressive ventricular hypertrophy and dilation in TNF TG mice are accompanied by a significant increase in MMP-2 and MMP-9 activity, an increase in collagen synthesis, deposition, and denaturation, and a decrease in undenatured collagens [15]. Furthermore, treatment with the MMP inhibitor BB-94 significantly reduces ventricular fibrosis and hypertrophy, and prolongs the survival of TNF TG mice [28]. In the present study, NF-κB KO selectively abrogated induction of MMP-9 in TNG TG myocardium. Since targeted deletion of MMP-9 has been shown to attenuate left ventricular enlargement and collagen accumulation after experimental myocardial infarction [35], the selective inhibition of MMP-9 might contribute to cardioprotective effects of NF-κB KO on TNF TG mice.

In the present study, we have demonstrated that the blockade of NF-κB activation prevents ventricular hyper-

trophy and remodeling in TNF-α-induced cardiomyopathy. However, the beneficial effects of NF-κB KO were limited to male TNF TG mice. The better survival function of female TNF TG mice might mask the beneficial effects of NF-κB KO. Gender difference in the survival of TNF TG mice has been repeatedly observed in our previous studies [12,13]. Echocardiographic analysis has demonstrated that impairment of baseline myocardial contractility and attenuation of β-adrenergic inotropic responsiveness are less severe in female TG mice [12]. Since the extent of myocardial expression of TNF-α has been shown to be comparable in both sexes, the gender difference is probably due to lower expression of TNF receptors in the myocardium of female TG mice [12]. Although we had hypothesized that activation of NF-κB might be less in female TG mice, our preliminary study suggests no apparent gender difference in the activation of NF-κB (data not shown). If the activation of NF-κB is similar between male and female TG mice, mechanisms by which female TG mice are protected from toxic effects of NF-κB activation remain to be determined. The role of NF-κB may be different between males and females.

Nonetheless, an inhibition of NF-κB may be a promising therapeutic strategy for cardiac remodeling and heart failure, especially when proinflammatory cytokines are activated. However, it might be undesirable to adopt systemic inhibition of NF-κB when we consider clinical application. Although NF-κB (p50) KO mice we used in the present study show no developmental abnormalities, they exhibit multifocal defects in immune responses involving B lymphocytes and nonspecific responses to infection; B cells do not proliferate in response to bacterial lipopolysaccharide and are defective in basal and specific antibody production [21]. Furthermore, inhibition of NF-κB activation in macrophages has been shown to increase atherosclerosis in LDL receptor-deficient mice, suggesting that systemic inhibition of NF-κB may promote vascular injury and atherosclerosis [36]. Although we did not detect any adverse events or premature death as long as we observed, systemic inhibition of NF-κB may be deleterious in the long run. Therefore, it might be better to develop a new technique to ensure cardiac-specific inhibition of NF-κB.

In conclusion, targeted disruption of the p50 subunit of NF-κB did not ameliorate myocardial inflammation but improved cardiac function and survival in male TNF TG mice. An inhibition of NF-κB may be a new therapeutic strategy for cardiac remodeling and heart failure, especially when proinflammatory cytokines are activated.

Acknowledgement

A part of this study was conducted in Kyushu University Station for Collaborative Research. This study was supported by a grant from Kimura Memorial Heart Foundation, by the Grant for Research on Cardiovascular Disease from Japan Heart Foundation/Pfizer Pharmaceuticals Inc., and by the Grant-in-Aid for Scientific Research from the Japan Society for the promotion of Science (C15590755).

References

[1] Wang H, Czura C, Tracey K. Tumor necrosis factor. In: Thomson A, Lotze M, editors. The cytokine handbook, 4th ed. San Diego: Academic Press; 2003. p. 837–60.
[2] Levine B, Kalman J, Mayer L, Fillit HM, Packer M. Elevated circulating levels of tumor necrosis factor in severe chronic heart failure. N Engl J Med 1990;323:236–41.
[3] Kubota T, McNamara DM, Wang JJ, Trost M, McTiernan CF, Mann DL, et al. Effects of tumor necrosis factor gene polymorphisms on patients with congestive heart failure. VEST investigators for TNF genotype analysis. Vesnarinone survival trial. Circulation 1998;97: 2499–501.
[4] Torre-Amione G, Kapadia S, Lee J, Durand JB, Bies RD, Young JB, et al. Tumor necrosis factor-alpha and tumor necrosis factor receptors in the failing human heart. Circulation 1996;93:704–11.
[5] Kubota T, Miyagishima M, Alvarez RJ, Kormos R, Rosenblum WD, Demetris AJ, et al. Expression of proinflammatory cytokines in the failing human heart: comparison of recent-onset and end-stage congestive heart failure. J Heart Lung Transplant 2000;19:819–24.
[6] Finkel MS, Oddis CV, Jacob TD, Watkins SC, Hattler BG, Simmons RL. Negative inotropic effects of cytokines on the heart mediated by nitric oxide. Science 1992;257:387–9.
[7] Yokoyama T, Vaca L, Rossen RD, Durante W, Hazarika P, Mann DL. Cellular basis for the negative inotropic effects of tumor necrosis factor-a in the adult mammalian heart. J Clin Invest 1993; 92:2012–303.
[8] Yokoyama T, Nakano M, Bendnarczyk JL, McIntyre BW, Entman M, Mann DL. Tumor necrosis factor-a provokes a hypertrophic growth response in adult cardiac myocytes. Circulation 1997;95:1247–52.
[9] Nakamura K, Fushimi K, Kouchi H, Mihara K, Miyazaki M, Ohe T, et al. Inhibitory effects of antioxidants on neonatal rat cardiac myocyte hypertrophy induced by tumor necrosis factor-alpha and angiotensin II. Circulation 1998;98:794–9.
[10] Krown KA, Page MT, Nguyen C, Zechner D, Gutierrez V, Comstock KL, et al. Tumor necrosis factor alpha-induced apoptosis in cardiac myocytes. Involvement of the sphingolipid signaling cascade in cardiac cell death. J Clin Invest 1996;98:2854–65.
[11] Kubota T, McTiernan CF, Frye CS, Slawson SE, Lemster BH, Koretsky AP, et al. Dilated cardiomyopathy in transgenic mice with cardiac-specific overexpression of tumor necrosis factor-alpha. Circ Res 1997;81:627–35.
[12] Kadokami T, McTiernan CF, Kubota T, Frye CS, Feldman AM. Sex-related survival differences in murine cardiomyopathy are associated with differences in TNF-receptor expression. J Clin Invest 2000;106: 589–97.
[13] Funakoshi H, Kubota T, Kawamura N, Machida Y, Feldman AM, Tsutsui H, et al. Disruption of inducible nitric oxide synthase improves beta-adrenergic inotropic responsiveness but not the survival of mice with cytokine-induced cardiomyopathy. Circ Res 2002;90: 959–65.
[14] Kubota T, Bounoutas GS, Miyagishima M, Kadokami T, Sanders VJ, Bruton C, et al. Soluble tumor necrosis factor receptor abrogates myocardial inflammation but not hypertrophy in cytokine-induced cardiomyopathy. Circulation 2000;101:2518–25.
[15] Li YY, Feng YQ, Kadokami T, McTiernan CF, Draviam R, Watkins SC, et al. Myocardial extracellular matrix remodeling in transgenic mice overexpressing tumor necrosis factor alpha can be modulated by anti-tumor necrosis factor alpha therapy. Proc Natl Acad Sci U S A 2000;97:12746–51.

[16] Bryant D, Becker L, Richardson J, Shelton J, Franco F, Peshock R, et al. Cardiac failure in transgenic mice with myocardial expression of tumor necrosis factor-alpha. Circulation 1998;97:1375–81.
[17] Barnes PJ, Karin M. Nuclear factor-kappaB: a pivotal transcription factor in chronic inflammatory diseases. N Engl J Med 1997;336: 1066–71.
[18] Purcell NH, Molkentin JD. Is nuclear factor kappaB an attractive therapeutic target for treating cardiac hypertrophy? Circulation 2003; 108:638–40.
[19] Purcell NH, Tang G, Yu C, Mercurio F, DiDonato JA, Lin A. Activation of NF-kappa B is required for hypertrophic growth of primary rat neonatal ventricular cardiomyocytes. Proc Natl Acad Sci U S A 2001;98:6668–73.
[20] Hirotani S, Otsu K, Nishida K, Higuchi Y, Morita T, Nakayama H, et al. Involvement of nuclear factor-kappaB and apoptosis signal-regulating kinase 1 in G-protein-coupled receptor agonist-induced cardiomyocyte hypertrophy. Circulation 2002;105:509–15.
[21] Sha WC, Liou HC, Tuomanen EI, Baltimore D. Targeted disruption of the p50 subunit of NF-kappa B leads to multifocal defects in immune responses. Cell 1995;80:321–30.
[22] Kubota T, Miyagishima M, Frye CS, Alber SM, Bounoutas GS, Kadokami T, et al. Overexpression of tumor necrosis factor-alpha activates both anti- and pro-apoptotic pathways in the myocardium. J Mol Cell Cardiol 2001;33:1331–44.
[23] Haudek SB, Bryant DD, Giroir BP. Differential regulation of myocardial NF kappa B following acute or chronic TNF-alpha exposure. J Mol Cell Cardiol 2001;33:1263–71.
[24] Shiomi T, Tsutsui H, Ikeuchi M, Matsusaka H, Hayashidani S, Suematsu N, et al. Streptozotocin-induced hyperglycemia exacerbates left ventricular remodeling and failure after experimental myocardial infarction. J Am Coll Cardiol 2003;42:165–72.
[25] Machida Y, Kubota T, Kawamura N, Funakoshi H, Ide T, Utsumi H, et al. Overexpression of tumor necrosis factor-alpha increases production of hydroxyl radical in murine myocardium. Am J Physiol Heart Circ Physiol 2003;284:H449.
[26] Hayashidani S, Tsutsui H, Ikeuchi M, Shiomi T, Matsusaka H, Kubota T, et al. Targeted deletion of MMP-2 attenuates early LV rupture and late remodeling after experimental myocardial infarction. Am J Physiol Heart Circ Physiol 2003;285:H1229.
[27] Janczewski AM, Kadokami T, Lemster B, Frye CS, McTiernan CF, Feldman AM. Morphological and functional changes in cardiac myocytes isolated from mice overexpressing TNF-alpha. Am J Physiol Heart Circ Physiol 2003;284:H960–9.
[28] Li YY, Kadokami T, Wang P, McTiernan CF, Feldman AM. MMP inhibition modulates TNF-alpha transgenic mouse phenotype early in the development of heart failure. Am J Physiol Heart Circ Physiol 2002;282:H983–9.
[29] Morishita R, Sugimoto T, Aoki M, Kida I, Tomita N, Moriguchi A, et al. In vivo transfection of *cis* element "decoy" against nuclear factor-kappaB binding site prevents myocardial infarction. Nat Med 1997;3:894–9.
[30] Lawrence T, Gilroy DW, Colville-Nash PR, Willoughby DA. Possible new role for NF-kappaB in the resolution of inflammation. Nat Med 2001;7:1291–7.
[31] Aizawa K, Suzuki T, Kada N, Ishihara A, Kawai-Kowase K, Matsumura T, et al. Regulation of platelet-derived growth factor-A chain by Krüppel-like factor 5: new pathway of cooperative activation with nuclear factor-kappaB. J Biol Chem 2004;279:70–6.
[32] Shindo T, Manabe I, Fukushima Y, Tobe K, Aizawa K, Miyamoto S, et al. Kruppel-like zinc-finger transcription factor KLF5/BTEB2 is a target for angiotensin II signaling and an essential regulator of cardiovascular remodeling. Nat Med 2002;8:856–63.
[33] Spinale FG. Matrix metalloproteinases: regulation and dysregulation in the failing heart. Circ Res 2002;90:520–30.
[34] Li YY, Feldman AM, Sun Y, McTiernan CF. Differential expression of tissue inhibitors of metalloproteinases in the failing human heart. Circulation 1998;98:1728–34.
[35] Ducharme A, Frantz S, Aikawa M, Rabkin E, Lindsey M, Rohde LE, et al. Targeted deletion of matrix metalloproteinase-9 attenuates left ventricular enlargement and collagen accumulation after experimental myocardial infarction. J Clin Invest 2000;106:55–62.
[36] Kanters E, Pasparakis M, Gijbels MJ, Vergouwe MN, Partouns-Hendriks I, Fijneman RJ, et al. Inhibition of NF-kappaB activation in macrophages increases atherosclerosis in LDL receptor-deficient mice. J Clin Invest 2003;112:1176–85.

Available online at www.sciencedirect.com
SCIENCE DIRECT®
Journal of Molecular and Cellular Cardiology 39 (2005) 231–239
Journal of Molecular and Cellular Cardiology
www.elsevier.com/locate/yjmcc

Original article

Contractile dysfunction of cardiomyopathic hamster myocytes is pronounced under high load conditions

Satoshi Nishimura [a], Hiroshi Yamashita [a], Masayoshi Katoh [a], Kelly P. Yamada [b], Kenji Sunagawa [c], Yasutake Saeki [d], Yosiki Ohnuki [d], Ryozo Nagai [a], Seiryo Sugiura [b,*]

[a] *The Department of Cardiovascular Medicine, Graduate School of Medicine, The University of Tokyo, Tokyo, Japan*
[b] *Computational Biomechanics Laboratory, The Institute of Environmental Studies, Graduate School of Frontier Sciences, The University of Tokyo, Hongo 7-3-1, Bunkyo-ku, Tokyo 113-0033, Japan*
[c] *The Department of Cardiovascular Medicine, Graduate School of Medicine, Kyushu University, Fukuoka, Japan*
[d] *Department of Physiology, Tsurumi University Dental School, Yokohama, Japan*

Received 12 October 2004; received in revised form 11 March 2005; accepted 30 March 2005

Available online 23 May 2005

Abstract

To understand the pathophysiology of hereditary cardiomyopathy, the contractile function of cardiomyopathic hamsters has been studied at the cellular level. However, most of the studies to date have described the cell shortening under the unloaded condition. Using a novel force–length measurement system for single cardiomyocytes, we studied the contractile function of cardiomyopathic hamster myocytes over a wide range of loading conditions. Cardiomyocytes were isolated from the ventricles of eight- to 10-week-old cardiomyopathic (CMP) hamsters (Bio TO-2 strain), as well as control (CTRL) Syrian hamsters. A pair of carbon fibers was attached to both ends of single cardiomyocytes and their contractile characteristics were recorded while changing the after-load by controlling the fiber motion. Under the unloaded condition, the shortening fraction (CMP 9.2 ± 0.5% vs. CTRL 10.7 ± 0.8%, $P = 0.06$) and maximum shortening velocity (CMP 98.2 ± 7.3 μm/s vs. CTRL 147.2 ± 6.5 μm/s, $P < 0.05$) were decreased in CMP hamster myocytes. The peak force under the isometric condition (CMP 35.8 ± 2.2 mN/mm^2 vs. CTRL 69.0 ± 8.4 mN/mm^2, $P < 0.05$) and external work (CMP 898 ± 130 J/m^3 vs. CTRL 3058 ± 576 J/m^3, $P < 0.05$) under physiologically loaded conditions were also decreased, but the differences were more pronounced under the loaded conditions. Calcium transients measured by Indo-1 revealed elevated diastolic level, decreased peak level, and slower diastolic decay in CMP myocytes thus being consistent with the observed contractile dysfunction. These results clearly indicate the importance of the loading conditions in evaluating the contractile function of CMP hamster myocytes, and may provide insights into the mechanism of contractile dysfunction in this disease.

Keywords: Cardiomyopathic hamster; Bio TO-2 strain; Cardiomyocyte; Isometric force; Calcium transient

1. Introduction

Cardiomyopathic Syrian hamsters have been used as models of hereditary cardiomyopathy and congestive heart failure. Most of the currently available strains are derived from the Bio 14.6 strain, and thus share the common genetic abnormalities identified in the exon of delta-sarcoglycan [1]. However, each strain presents a distinct phenotype depending on the stage of life. For example, some strains show significant cardiac hypertrophy in the early stage of disease (Bio 14.6, UM-X7.1 and CHF 146), whereas others (Bio 53.58 and Bio TO-2) are characterized by prominent dilation of the ventricles without wall hypertrophy [1–3].

To understand the pathogenesis of these animal models and the pathophysiology of heart failure, many studies have been undertaken at the organ [4], tissue [5,6] and cellular [7–11] levels to identify changes in the ion currents [6,11], action potentials [5], calcium kinetics [5,7,10] and mechanical properties [4,6,10]. Among these, studies on mechanics using isolated single cardiomyocytes have the advantage of establishing a direct link between subcellular abnormalities and mechanical properties by eliminating extracellular factors such as fibrosis, which is known to develop in cardiomyopathic tissue. However, most of the studies [7,10,12] in this

* Corresponding author. Tel./fax: +81 3 5841 8393.
E-mail address: sugiura@k.u-tokyo.ac.jp (S. Sugiura).

0022-2828/$ - see front matter © 2005 Elsevier Ltd. All rights reserved.
doi:10.1016/j.yjmcc.2005.03.022

field have evaluated the mechanical properties of cardiomyopathic myocytes under unloaded or light load conditions, and are far from the actual situation where the failing heart is working against high after-load and/or preload. Recently, we developed a novel force–length measurement system for isolated single cardiomyocytes using carbon fibers [13,14]. Using this system, in which the motion of the carbon fibers is controlled by a piezo-electric device, we can study the mechanics of a single cardiomyocyte over a wide range of loading conditions, including unloaded, isometric and physiologically loaded conditions.

Accordingly, the purpose of this study was to evaluate the mechanics of single cardiomyocytes isolated from cardiomyopathic hamsters (Bio TO-2 strain) in the early and compensated phases under a wide range of loading conditions. The results clearly revealed that the functional impairment became evident under high load, indicating the importance of functional analysis under loaded conditions. The underlying mechanism for the contractile dysfunction will also be discussed.

2. Materials and methods

2.1. Animals and myocyte isolation

All experiments were conducted in accordance with the National Research Council "Guide for the Care and Use of Laboratory Animals" and approved by our Institutional Animal Care and Use Committee. Eight- to 10-week-old male Syrian cardiomyopathic (CMP) hamsters (Bio TO-2 strain) and age-matched Syrian golden hamsters (control: CTRL) were obtained from the Bio-Breeders Institute (Cambridge, MA). We chose to use the hamsters at this relatively young age because Bio TO-2 strain hamsters are known to show cardiac dysfunction (low cardiac output) at this stage of life without developing significant interstitial fibrosis. The influence of fibrosis on myocyte isolation and functional analysis will be discussed later (Section 4.1).

The hamsters were anesthetized with an intraperitoneal injection of pentobarbital (500 mg/kg body wt.). After anticoagulation with heparin (10,000 U/kg i.p.) the heart was quickly removed and retrograde perfusion was initiated with nominally Ca^{2+}-free HEPES-Tyrode solution (130 mM NaCl, 5.4 mM KCl, 0.5 mM $MgCl_2$, 0.33 mM NaH_2PO_4, 22 mM glucose, 5 mM glutamine, 0.4 mM EGTA, 25 mM HEPES, pH 7.4) at 37 °C. After 5 min, the perfusate was switched to an enzyme solution containing collagenase (1 mg/ml Collagenase Type 2; Worthington), protease (0.05 mg/ml Type XIV; Sigma) and trypsin (0.05 mg/ml; Sigma) and maintained for 20 min. Finally, the enzyme was washed out by perfusion and the calcium concentration of the Tyrode solution was gradually increased to 1.1 mM. The isolated myocytes were then transferred to an experimental chamber, the glass bottom of which was coated with poly-HEME (2-hydroxyethyl methacrylate; Sigma) to prevent adhesion of the myocytes during the force and length measurements.

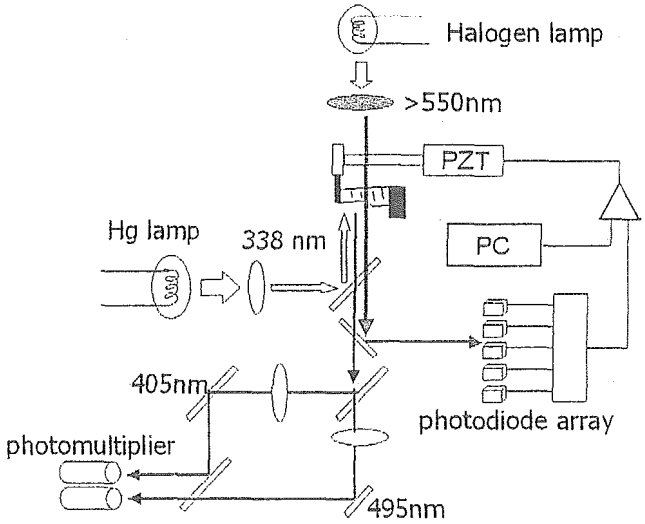

Fig. 1. Diagram of the experimental setup. The position of the fiber is detected by a photodiode array. The position signal is processed by a PC, and the calculated command signal is applied to a piezo-electric translator (PZT) connected to the carbon fiber. To observe the ratiometric Indo-1 signal, the myocytes are illuminated by a high-pressure mercury-arc lamp (excitation 338 nm) and the fluorescent light is divided by a dichroic beam splitter in order to measure two peaks of fluorescence (405 and 495 nm) simultaneously using two photomultiplier tubes.

2.2. Measurement of the force and length relationships

The principle of the single cardiomyocyte force–length measurement system has been described previously [13–15]. Briefly, a single cardiomyocyte was selected under a microscope according to the following criteria: 1) a rod shape with an average sarcomere length of > 1.65 μm (measured by on-line Fourier analysis of optical density traces of the sarcomere pattern of the myocyte image; SarcLen, IonOptix, Milton, MA); and 2) greater than 5% contraction of the total myocyte length in response to electrical stimulation. Next, a pair of carbon fibers was attached to each end of the selected myocyte using micromanipulators. One of the fibers was thin and compliant (diameter 7 μm, stiffness 80–200 nN/μm), while the other was thick and rigid (diameter 30 μm, stiffness > 1000 nN/μm) and served as a mechanical anchor. The image of the compliant fiber was projected onto a linear 1024-element photodiode array (S3903; Hamamatsu Photonics, Japan) to monitor the bending motion induced by active contraction or passive stretching (Fig. 1). Furthermore, we controlled the position of the compliant fiber by moving a piezo-electric translator (PZT) (P-841.40; Physik Instrumente, Germany) that was connected to it. Myocyte length signals obtained by the photodiode array sensor were sampled and processed at 1 kHz, and the generated command signal was applied to the PZT driver with a 16 bit A/D, D/A converter (6035E; National Instruments, TX) connected to a personal computer (PC). The myocyte was electrically stimulated at 0.5 Hz with pulses of 10 ms duration. Before the force measurements, we stretched the diastolic myocyte length to 105% of the slack length while measuring the sarcomere length (IonOptix). All experiments were performed at 37 °C (Thermo-

plate; TOKAIHIT, Japan). By controlling the motion of the PZT with the adaptive control system, we measured the contractile function under isometric, unloaded and physiologically loaded conditions in each myocyte. The cross-sectional area of the myocyte was estimated from videotaped images assuming an elliptical cross-section with a long-to-short axis ratio of 1:3.

2.3. Ca^{2+} transients

To record intracellular calcium transients, myocytes were incubated at room temperature in culture medium containing Indo-1-AM (1 μM; Wako, Japan) and Pluronic F127 (0.004%; Sigma) for 15 min. The myocytes were illuminated via epifluorescence optics (40× objective; UPlan Apo, Olympus, Tokyo) using a high-pressure mercury-arc lamp (excitation 338 nm) and the fluorescent light was divided by a dichroic beam splitter to permit simultaneous measurement of two peaks of Indo-1 fluorescence (405 and 495 nm) using two separate photomultiplier tubes. The myocytes were paced at 0.5 Hz. After confirming the stability in fluorescent signals of calcium transients (usually 5–10 s), the $[Ca^{2+}]_i$ was recorded. The data were averaged for consecutive two beats. After measurement of the intracellular calcium transients, the myocytes were permeabilized to Ca^{2+} by treatment with 25 μM digitonin (Sigma) under zero Ca^{2+} (10 mM EGTA) or 1 mM Ca^{2+} conditions to obtain the calibration factors R_{min}, R_{max} and beta. From these values $[Ca^{2+}]_i$ was calculated by $[Ca^{2+}]_i = K_d\,[(R - R_{min})/(R_{max} - R)]$ beta, using $K_d = 250$ nM as described in Ref. [16].

2.4. Myosin isoforms

The myosin isoform distributions of the right and left ventricular tissues from both CMP and CTRL hamsters were determined by pyrophosphate gel electrophoresis according to Martin et al. [17]. Myocardial tissue was obtained during the course of myocyte isolation, and then quickly frozen at –85 °C and thawed before processing. For each sample, equal amounts of tissue were homogenized and loaded onto the gel. After staining, the gels were analyzed using a scanning densitometer (LKB 2202; LKB Produkter, Sweden).

2.5. Data analysis

All the data were sampled at 1 kHz and recorded by an A/D converter connected to a PC (MacLab 8s; ADInstruments, Australia). The results are expressed as mean ± S.E.M., and differences between CMP and CTRL were tested for statistical significance by Student's *t*-test for unpaired data. *P* values < 0.05 were considered significant.

3. Results

3.1. Myocyte isolation and morphology

Although not significant, we observed interstitial fibrosis in the CMP ventricular tissue, which may have influenced the isolation procedure. However, we were able to collect myocytes from both CMP and CTRL ventricles with equally good viability, i.e. 90% of the myocytes were rod-shaped and responded stably to electrical stimulation. From these observations, we considered that there was no selection bias in the isolation procedure.

There were no obvious morphological differences between the cardiomyocytes isolated from CMP and CTRL hamsters (data not shown), except for the significantly shorter diastolic sarcomere length of CMP myocytes (CMP 1.72 ± 0.03 μm vs. CTRL 1.90 ± 0.02 μm, $P < 0.05$). We did not observe any width difference between the myocytes, in contrast to previous reports [10,18,19].

3.2. Force and length relationships

Eleven control myocytes and 10 cardiomyopathic myocytes were studied (Table 1). For each myocyte, we recorded the force–length relationships under a wide range of loading conditions, including isometric, unloaded and physiologically loaded conditions. A series of the force–length loops obtained under a wide range of loading conditions are shown for single myocytes from CTRL (Fig. 2A) and CMP (Fig. 2B) hamsters.

Under the unloaded condition, CMP myocytes shortened by 9.2 ± 0.5% of the myocyte length, which was lower than that for CTRL myocytes (10.7 ± 0.8%, $P = 0.06$), but the difference did not reach statistically significant. Similarly, the maximal shortening velocity (V_{max}) was significantly lower in CMP myocytes (CMP 98.2 ± 7.3 μm/s vs. CTRL 147.2 ± 6.5 μm/s, $P < 0.05$) (Table 1 and Fig. 3).

Fig. 4 shows time courses of the force (Fig. 4A) and length (Fig. 4B) changes of CTRL (solid line) and CMP (broken line) myocytes under the isometric condition. The length change was less than 0.5 μm for both groups. On average, the peak force of CTRL myocytes was 5.40 ± 0.64 μN (69.0 ± 8.4 mN/mm^2 for the cross-sectional area), which was comparable to the previously reported values for single rat ventricular myocytes [14,20,21] and papillary muscle preparations [5,6,22]. In CMP myocytes, the peak force was significantly decreased to 3.22 ± 0.24 μN (35.8 ± 2.2 mN/mm^2, $P < 0.05$). The relative reduction in the peak force was 48.0% compared to the CTRL value, and thus far greater than the relative reduction in the contractile indices obtained under the unloaded condition (shortening fraction 14.0%, V_{max} 33.3%) (Fig. 3A–C). We also found that the time course of contraction under the unloaded condition was significantly prolonged in CMP myocytes (time to half relaxation: CMP 41.5 ± 2.9 ms vs. CTRL 32.3 ± 2.7 ms, $P < 0.05$.)

When we simulated a physiological working condition consisting of isometric contraction followed by shortening and isometric relaxation (Fig. 2A, B), the average external work outputs calculated as the area circumscribed by the force–length loop were 898 ± 130 J/m^3 for CMP myocytes and 3058 ± 576 J/m^3 for CTRL myocytes. In this analysis, the difference in performance between the two groups was further accentuated (70.6% relative reduction) (Fig. 3D).

Table 1
Contractile functions of control and cardiomyopathic hamster myocytes under unloaded, isometric and physiologically loaded conditions

Control	Shortening under unloaded conditions			Force under isometric conditions		Physiologically loaded conditions		
	Length (%)	Vmax (μm/s)	RT1/2 (ms)	Force (μN)	Force (mN/mm2)	Work area (J/m2)	Slope of linear regression (nN/μm)	Sarcomere length (μm)
1	12.4	174	34	7.00	89.1	2629	1053	1.81
2	12.3	173	47	9.72	68.6	3088	2975	1.78
3	8.7	136	40	5.68	55.3	2420	1701	1.84
4	10.0	130	27	6.20	115.0	6791	2596	1.95
5	9.2	121	20	6.15	36.9	1132	1530	1.78
6	16.0	153	34	4.73	53.9	3005	797	2.01
7	12.1	173	35	3.51	50.2			1.93
8	10.0	123	28	2.76	59.0			1.96
9	7.8	139	37	3.90	52.6			1.98
10						2890		1.88
11	8.8	150	21	4.37	109.0	2506	647	1.94
Mean	10.7	147.2	32.3	5.40	69.0	3058	1614	1.90
S.E.M.	0.8	6.5	2.7	0.64	8.4	576	336	0.02
Cardiomyopathic hamsters								
1	7.8	99	38	4.04	34.0	312	314	1.66
2	9.1	81	42	2.34	40.6	1555	500	1.89
3	10.0	100	37	3.68	44.3	844	1041	1.67
4	10.8	121	63	2.16	40.1	716	398	1.67
5	11.2	136	41	4.16	40.5	1220	793	1.68
6	10.8	83	35	2.99	38.0	1169	525	1.83
7	6.3	60	41	2.71	30.8	367	659	1.73
8	7.8	119	50	4.15	30.6	1215	974	1.66
9	8.6	105	29	3.24	39.0	1053	662	1.67
10	10.1	78	39	2.73	20.1	534	593	1.73
Mean	9.2	98.2	41.5	3.22	35.8	898	646	1.72
S.E.M.	0.5	7.3	2.9	0.24	2.2	130	74	0.03

In a previous report, we showed that the curve connecting the upper left corners of force–length loops obtained under a wide range of loading conditions shifted upward and left in response to positive inotropic interventions, analogous to the end–systolic pressure–volume relationship in the rodent ventricle [14]. Applying linear regression to these points yielded slopes of 646 ± 74 nN/μm in CMP myocytes and 1614 ± 336 nN/μm in CTRL myocytes. The difference between the slopes for CMP and CTRL was also statistically significant ($P < 0.05$), thus confirming the depressed contractility of CMP myocytes.

In four myocytes for both CTRL and CMP, we measured the passive force–sarcomere–length relations as shown in Fig. 5A. Acquired curves were fitted to the following exponential function, $y = e^{\frac{x-a}{b}} - 1$, where b characterizes the curvature. We found that the constant a was significantly different between CMP (1.72 ± 0.01 μm, $n = 4$), and CTRL (1.87 ± 0.02 μm, $n = 4$), ($P > 0.05$), whereas constant b was not (CMP 0.081 ± 0.014, $n = 4$, and CTRL 0.058 ± 0.008, $n = 4$, $P = 0.10$). To elucidate the cause of this leftward shift in passive force–sarcomere–length relation, we repeated the

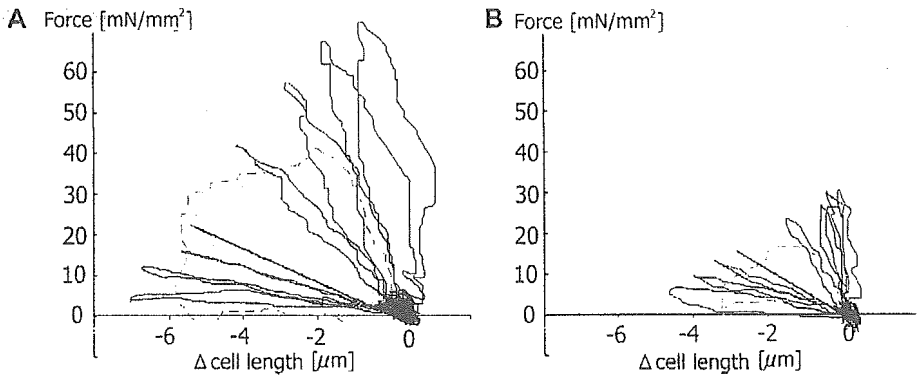

Fig. 2. Force–length loops of single cardiomyocytes under various loading conditions. Data for control (A) and CMP (B) hamster myocytes are shown. The ordinate shows myocyte length, and the abscissa shows force per cross-sectional area. In each panel, the broken line shows the loop under physiologically loaded conditions.

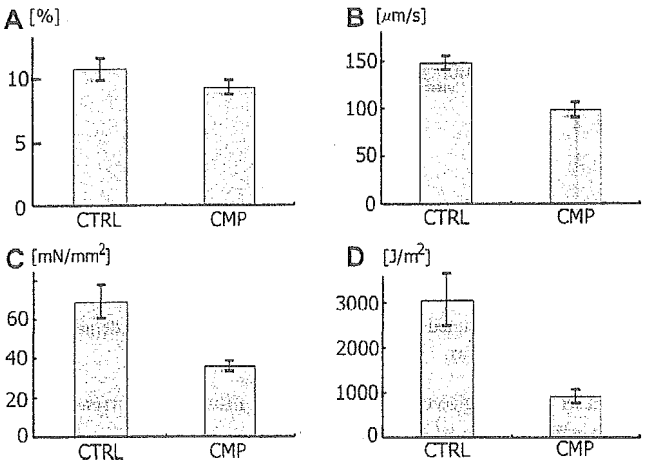

Fig. 3. Comparison of the contractile function between CMP and CTRL hamster myocytes. The shortening fraction (A) and velocity (B) under unloaded condition, isometric force (C) under isometric, and external work (D) under physiologically unloaded condition are shown. The values are mean ± S.E.M.

measurement for another three CMP and three CTRL myocytes in the presence of 20 mM 2,3-butanedione monoxime (BDM) (WAKO Chemicals, Japan) which is known to inhibit crossbridge formation [23]. Addition of BDM shifted the force–sarcomere–length relations of CMP myocytes rightward thereby made them close to those of CTRL (Fig. 5B) (CMP: $a = 1.86 \pm 0.03$ μm, $b = 0.077 \pm 0.016$, $n = 3$, CTRL: $a = 1.86 \pm 0.03$ μm, $b = 0.097 \pm 0.007$, $n = 3$).

3.3. Calcium transients

Fig. 6 shows recordings of $[Ca^{2+}]_i$ for CTRL (Fig. 6A, $n = 10$), and CMP (Fig. 6B, $n = 9$) myocyte. The peak calcium concentration was decreased in CMP cells (CMP 630.1 ± 60.6 nM vs. CTRL 805.5 ± 67.0 nM, $P < 0.05$), but the diastolic level increased (CMP 181.9 ± 32.4 nM vs. CTRL 113.4 ± 56.4 nM, $P < 0.05$). The time courses of intracellular Ca^{2+} transients were prolonged in CMP myocytes. In particular, the rate of diastolic $[Ca^{2+}]_i$ decay, as measured by the relaxation time required for half decay (RT1/2), was significantly slower in CMP myocytes (CMP 216.2 ± 13.3 ms vs. CTRL 117.1 ± 4.4 ms, $P < 0.05$).

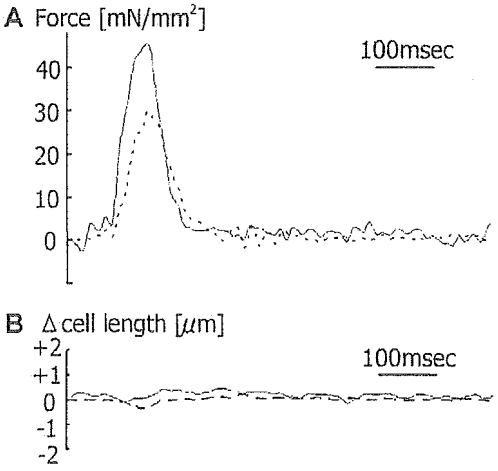

Fig. 4. Time courses of isometric contraction. Force (A) and length (B) changes for CMP (broken line) and CTRL (solid line) myocytes under the isometric condition are shown. Under the isometric condition, the length changes are less than 0.5 μm for both groups.

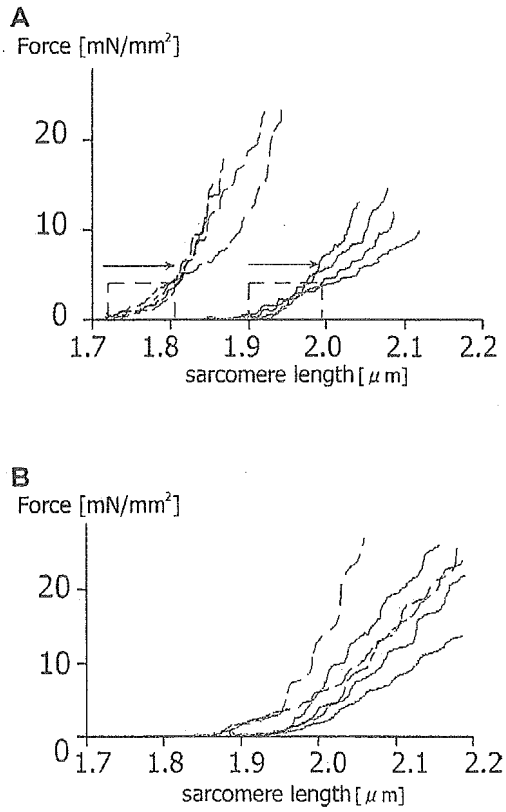

Fig. 5. A: Passive force-sarcomere length relations of CMP (broken line, $n = 4$) and CTRL (solid line, $n = 4$) myocytes. Stretching the cell to 105% of resting length (arrows and horizontal gray dotted lines) produced the same preload for both myocytes (vertical gray dotted lines). B: Passive force–sarcomere–length relations of CMP (broken line) and CTRL (solid line) myocytes in the presence of 20 mM BDM. BDM shifted the relations of CMP myocytes rightward to make them similar to those of CTRL.

3.4. Myosin isoforms

Ventricular myosin from CTRL hamsters showed a V_1 isoform predominance, whereas that from CMP hamsters showed a redistribution to V_2 and V_3 (Fig. 7) in both the left and right ventricles. When we quantified the isoform distribution by measuring the area under each peak and calculating the percentage of the α-myosin heavy chain (%α-MHC) using the formula $\%\alpha\text{-MHC} = \%V_1 + \%V_2/2$, the value was 66.3 ± 3.6% ($n = 3$) for CMP left ventricular myosin compared to 100% ($n = 3$) for CTRL.

4. Discussion

4.1. Selection of animal strain and age

In this study, we analyzed the contractile performance of single cardiomyocytes isolated from the cardiomyopathic

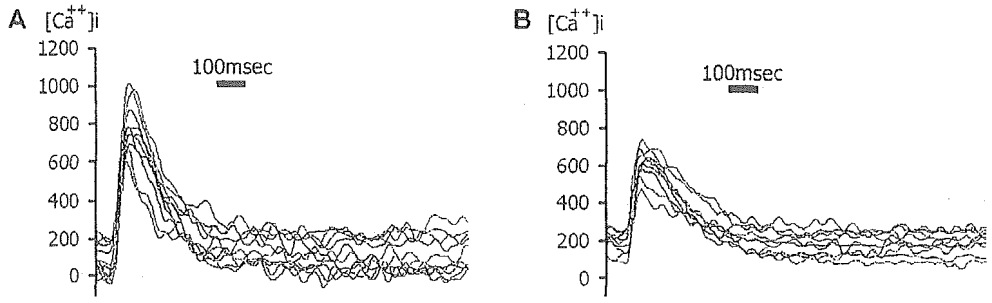

Fig. 6. Calcium transients of control (A, $n = 10$) and cardiomyopathic (B, $n = 9$) hamster myocytes calculated from the Indo-1 signal (see text for detail). The transient of CMP myocytes showed an elevated diastolic level, lower peak level, and slower diastolic decay.

hamster Bio TO-2 strain. Derived from the Bio 14.6 strain, a well-known animal model of hypertrophic cardiomyopathy, the Bio TO-2 strain shares a common defect in a gene for delta-sarcoglycan with the Bio 14.6 strain, but presents a distinct phenotype of dilated cardiomyopathy [24,25]. This difference in phenotype can be explained by the recent findings that the Bio 14.6 strain shows heterogeneously preserved alpha- and gamma-sarcoglycan with loss of beta- and delta-sarcoglycan, while Bio TO-2 strain hamsters do not show any sarcoglycans.

We selected the Bio TO-2 strain because this strain is relatively homogeneous in its clinical course, and the decrease in cardiac function (low cardiac output) starts earlier than the development of overt signs of congestive heart failure [4,6]. Furthermore, we chose to use 8-week-old hamsters, which are younger than those used in earlier studies (approximately 4 months–1 year) [7,9,10,18]. We chose this age because: 1) we may be able to detect early changes in function that are hardly modified by the compensatory mechanisms; and 2) we wanted to avoid any problems associated with cell isolation, since cardiomyopathic hamsters develop significant cardiac fibrosis which sometimes requires larger doses of proteases and longer incubation causing damage to the myocytes. Damaged myocytes tend to have calcium overload, as evidenced by their short sarcomere length, irregular shape and irritability, which may have an effect on comparisons with CTRL myocytes that are easily isolated and therefore less damaged. In many preliminary experiments, we identified the critical age limit for avoiding cell damage during the isolation procedure to be about 8 weeks. At this age, we succeeded in isolating over 90% viable (not damaged) myocytes from both CTRL and CMP hamsters.

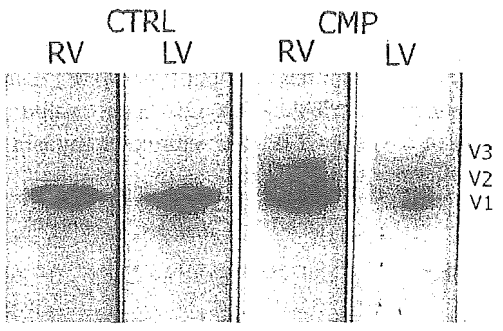

Fig. 7. Cardiac myosin isoforms. Pyrophosphate gels of cardiac myosin from the right ventricle (RV) and left ventricle (LV) of CTRL and CMP hamsters are shown. A redistribution from V_1 to V_2 and V_3 is observed in CMP myocytes.

4.2. *Effect of load on performance*

Using the novel force–length measurement system, we could evaluate the contractile function of single cardiomyocytes from CMP and CTRL hamsters over a wide range of loading conditions, including unloaded, isometric and physiological loading conditions.

Under the unloaded condition, we found a small difference in the shortening fraction and maximum shortening velocity between the two groups. There are only a few previous studies in which the shortening velocity and/or shortening fraction of single cardiomyocytes isolated from cardiomyopathic hamsters (Bio 14.6, CHF 146) have been discussed [7,9,10,12]. All of these studies unanimously showed a slower time course for contraction in cardiomyopathic hamsters, compatible with our results. Furthermore, the shortening fraction tended to be decreased in cardiomyopathic myocytes, although the differences were small under a low extracellular calcium concentration, also compatible with the present results.

To our knowledge, no data are available regarding the isometric twitch force for single cardiomyocytes from either normal or cardiomyopathic hamsters. However, since failing hearts are working against a high after-load in situ, evaluation of the contractile function under high load conditions is of great importance. Indeed, when we compared the isometric twitch forces of single cardiomyocytes from CTRL and CMP hamsters, we found that the difference in function was pronounced under high load conditions compared to the unloaded condition. A similar tendency was reported in a study using papillary muscle preparations, which showed a decreased tension-generating ability with a relatively maintained shortening velocity of the cardiomyopathic Syrian hamster myocardium [5]. Also in vivo condition, decreased mean arterial pressure and stroke volume have been reported for TO-2 hamsters [4]. The implications of these findings are twofold. First, the cardiomyopathic myocytes in congestive heart failure fail to match the high after-load and deteriorate further. Second, the subcellular mechanisms related to force generation may constitute the primary defect in this disease condition.

4.3. Mechanistic considerations

To gain insights into the mechanism of contractile dysfunction, we measured the calcium transients in both CTRL and CMP hamster myocytes. The results in previous reports have been conflicting. Hatem et al. [7] reported that the magnitudes of the peak intracellular calcium transients were similar between control and cardiomyopathic hamster myocytes, but the time courses were slower in the cardiomyopathic myocytes. Kruger et al. [18] reported significantly decreased peak calcium transients, whereas Sen et al. [10] reported higher time-averaged $[Ca^{2+}]_i$. Although the cause of these discrepancies is not clear, we consider that the distinct phenotype (various degree of cardiac hypertrophy or dilation) due to the different age and strain used in each study is an important factor. Our experiments were performed using younger (8 weeks of age) TO-2 strain compared to the previous reports using older (7–14 months of age) Bio 14.6 strain. The other possibility is the effect of temperature, since the experiments were performed at 37 °C in the current study and Sen et al. [10], 35 °C in Kruger et al. [18] and room temperature in Hatem et al. [7]. In this study, we observed the elevated diastolic level, decreased peak level, and slower diastolic decay of calcium transient in CMP myocytes. These changes in calcium transient were probably caused by the impairment of the sarcoplasmic reticulum function and could account for, at least in part, the shorter resting sarcomere length and impaired contractile function of CMP myocytes.

We also analyzed the myosin isoform distribution and found a shift from V_1 to V_2 and V_3 as reported in other cardiomyopathic strains [26,27]. The relationship between the myosin isoform composition and the maximum shortening velocity (V_{max}) has been studied extensively at the muscle [28,29], cellular [30] and molecular [31] levels. Using an in vitro motility assay technique, we showed that the sliding velocity of beads coated with myosin from CMP (Bio 14.6) hamster ventricles was dependent on the α-MHC content (%α-MHC) [32]. Consistent with that result, we found that the V_{max} of CMP myocytes with 66.3% α-MHC was about 70% of that of CTRL myocytes with 100% α-MHC in this study.

On the other hand, the influence of the myosin isoform redistribution on the force-generating ability of cardiac muscle is controversial and data are available only for other animal species. Using an in vitro force measurement system, VanBuren et al. [33] reported that V_3 myosin generated a greater force than V_1 myosin from rabbit, whereas Sugiura et al. [34] showed that the two myosins from rat had equal force-generating ability using a similar experimental system. The two myosins have also been suggested to have equal force-generating ability in rat papillary muscle preparations [35]. However, these results cannot add much to the explanation for the smaller force observed in the CMP hamster myocytes containing a greater amount of the V_3 myosin isoform.

Recent studies have identified mutations in the exon of delta-sarcoglycan in cardiomyopathic hamsters [1,36]. Since sarcoglycans are located in the sarcolemma as anchors connecting myofibrillar proteins to the sarcolemma via cytoskeletal proteins [37], abnormalities in these proteins can cause defects in transmission of the force generated by the contractile proteins to the extracellular matrix. The present finding that the contractile dysfunction of Bio TO-2 hamster myocytes is pronounced under high load may provide support for this hypothesis, although further studies are required to fully address this issue.

We also found that the passive force–sarcomere–length relations of cardiomyopathic myocytes were shifted leftward compared to the control indicating the stiffer passive property. We consider the crossbridge formation due to the elevated diastolic calcium level to be the major cause. Normalization of leftward shift by the BDM in cardiomyopathic myocytes strongly supported this hypothesis, but other factors should also be taken into account. We can find a paper reporting the stiff passive property of cardiomyopathic papillary muscle [5]. Although direct comparison was difficult, because sarcomere length was not measured in their study, passive property of our control myocytes were close to their control one. On the other hand, passive property of cardiomyopathic myocytes was stiffer compared to papillary muscle data. Extracellular collagen mesh exists in multi-cellular preparation but, as shown by Granzier and Irving [38], its contribution to the passive property is minimal in the short sarcomere length studied here. Alternatively, we speculate the other role of collagen mesh in modulating the experimentally determined passive property. In papillary muscle preparations, with the aid of collagen mesh, tensile stress applied at the ends could be distributed homogeneously over the sarcolemma and transmitted to each sarcomere through costameres. On the other hand, sarcomeres might not be stretched efficiently in cardiomyocyte by the force applied and concentrated at the edge of sarcolemma. In addition, as stated above, the defects in delta-sarcoglycan could impair the force transmission to sarcomere in CMP myocytes. In fact, loosening sarcomeres has been reported in the absence of cytoskeletal protein desmin connecting the Z-line in skeletal muscle [39].

In this study, comparison of contractile function was made at different sarcomere length between the two groups because of the following reasons. Upon isolation, resting sarcomere length was significantly shorter for CMP animals possibly due to the increased diastolic calcium concentration. Fig. 5 also shows that if we tried to stretch the sarcomere length of CMP myocytes to the same level with CTRL myocytes, it required abnormally high tension. Indeed, upon stretch of such degree, CMP myocyte contracted spontaneously probably due to the activation of stretch activated channel and hampered our measurement under steady-state condition. However, in the shorter sarcomere length range, where tension-sarcomere length relations were relatively linear and flat, so that the 5% stretch from the resting length (horizontal dotted lines in Fig. 5A) required comparable tension (preload) (vertical dotted lines in Fig. 5A) for both cases. For this reason, we made comparison at the constant preload by stretching the myocytes from both groups to 105% of resting length.

To further clarify the abnormality in excitation–contraction coupling of the cardiomyopathic myocytes, interventions such as changing pacing rate or giving inotropic agent would be useful. However, under such interventions, cardiomyopathic myocytes became highly irritable against stretch and started spontaneous irregular contractions. Unfortunately, we do not have any measures to circumvent this problem at present.

4.4. Summary

In summary, cardiomyocytes isolated from cardiomyopathic hamsters (Bio TO-2 strain) showed impaired contractile function compared to those from normal control hamsters, and the contractile dysfunction was pronounced in the indices obtained under high load conditions. These findings indicate the importance of evaluating myocyte function under high load and also provide suggestions for the pathogenesis of this disease condition.

Acknowledgements

We thank Ms. C. Miyazawa for her excellent technical assistance. This study was supported by grants from the Program for Promotion of Fundamental Studies in Health Sciences of the Organization for Pharmaceutical Safety and Research, the Vehicle Racing Commemorative Foundation, Suzuken Memorial Foundation and the Research Grant for Cardiovascular Disease from the Ministry of Health, Labour and Welfare. K.P.Y. was supported by a Grant-in-Aid for JSPS Fellows related to a JSPS Postdoctoral Fellowship for Foreign Researchers.

References

[1] Sakamoto A, Ono K, Abe M, Jasmin G, Eki T, Murakami Y, et al. Both hypertrophic and dilated cardiomyopathies are caused by mutation of the same gene, delta-sarcoglycan, in hamster: an animal model of disrupted dystrophin-associated glycoprotein complex. Proc Natl Acad Sci USA 1997;94:13873–8.

[2] Makino N, Masutomo K, Nshimura M, Maruyama T, Yanaga T. Cardiac collagen expression in the development of two types of cardiomyopathic hamsters (Bio. 14.6 and Bio 53.58. In: Nagano M, Takeda N, Dhalla NS, editors. THe cardiomyopathic heart. New York: Raven Press; 1994. p. 1–65.

[3] Panchal BC, Trippodo NC. Systemic and regional haemodynamics in conscious BIO TO-2 cardiomyopathic hamsters. Cardiovasc Res 1993;27:2264–9.

[4] Goineau S, Pape D, Guillo P, Ramée MP, Bellissant E. Hemodynamic and histomorphometric characteristics of dilated cardiomyopathy of Syrian hamsters (Bio TO-2 strain). Can J Phsyiol Phramacol 2001;79: 329–37.

[5] Capasso JM, Olivetti G, Anversa P. Mechanical and electrical properties of cardiomyopathic hearts of Syrian hamsters. Am J Physiol 1989;257:H1836–H1842.

[6] Antony I, Chemla D, Lecarpentier Y. Myocardial contractility, lusitropy and calcium responsiveness in young (50 days) and hypertrophied (180 days) cardiomyopathic hamsters. J Mol Cell Cardiol 1992;24(10):1089–100.

[7] Hatem SN, Sham JSK, Morad M. Enhanced Na^+–Ca^{2+} exchange activity in cardiomyopathic Syrian hamster. Circ Res 1994;74:253–61.

[8] Howlett SE, Bobet J, Gordon T. Force-interval relation in normal and cardiomyopathic hamster atria. Am J Physiol 1991;261:H1597–H1602.

[9] Sen L, O'neill M, Marsh JD, Smith TW. Inotropic and calcium kinetic effects of calcium channel agonist and antagonist in isolated cardiac myocytes from cardiomyopathic hamsters. Circ Res 1990;67:599–608.

[10] Sen L, O'neill M, Marsh JD, Smith TS. Myocyte structure, function, and calcium kinetics in the cardiomyopathic hamster heart. Am J Physiol 1990;259:H1533–H1543.

[11] Rossner KL. Calcium current in congestive heart failure of hamster cardiomyopathy. Am J Physiol 1991;260:H1179–H1186.

[12] Howlett SE, Xiong W, Mapplebeck CL, Ferrier GR. Role of voltage-sensitive release mechanisms in depression of cardiac contraction in myopathic hamsters. Am J Physiol 1999;277:H1690–H1700.

[13] Yasuda S, Sugiura S, Kobayakawa N, Fujita H, Yamashita H, Katoh K, et al. A novel method to study contraction characteristics of a single cardiac myocyte using carbon fibers. Am J Physiol Heart Circ Physiol 2001;281(3):H1442–H1446.

[14] Nishimura S, Yasuda S, Katoh M, Yamada KP, Yamashita H, Saeki Y, et al. Single cell mechanics of rat cardiomyocytes under isometric, unloaded and physiologically loaded conditions. Am J Physiol 2004; 287:H196–H202.

[15] Yasuda S, Sugiura S, Yamashita H, Nishimura S, Saeki Y, Momomura S, et al. Unloaded shortening increases the peak of Ca^{2+} transients but accelerates their decay in rat single cardiac myocytes. Am J Physiol 2003;285:H470–H475.

[16] Ikenouchi H, Peters GA, Barry WH. Evidence that binding of indo-1 to cardiac myocyte protein does not markedly change K_d for Ca^{2+}. Cell Calcium 1991;12:415–22.

[17] Martin AF, Pagani ED, Solaro RJ. Thyroxine-induced redistribution of isozymes of rabbit ventricular myosin. Circ Res 1982;50:117–24.

[18] Kruger C, Erdman E, Nabauer M, Beuckelmann DJ. Intracellular calcium handling in isolated ventricular myocytes from cardiomyopathic hamsters (strain BIO 14.6) with congestive heart failure. Cell Calcium 1994;16:500–8.

[19] Sorenson AL, Tepper D, Sonnenblick EH, Robinson TF, Capasso JM. Size and shape of enzymatically isolated ventricular myocytes from rats and cardiomyopathic hamsters. Cardiovasc Res 1985;19(12): 793–9.

[20] Bluhm WF, McCulloch AD, Lew WY. Active force in rabbit ventricular myocytes. J Biomech 1995;28(9):1119–22.

[21] Palmer RE, Brady AJ, Roos KP. Mechanical measurement from isolated cardiac myocytes using a pipette attachment system. Am J Physiol 1996;270:C697–C704.

[22] Janssen PM, de Tombe PP. Uncontrolled sarcomere shortening increases intracellular Ca^{2+} transient in rat cardiac trabeculae. Am J Physiol 1997;272(4 Pt 2):H1892–H1897.

[23] Backx PH, Gao WD, Azan-Backx MD, Marban E. Mechanism of force inhibition by 2,3-butanedione monoxime in rat cardiac muscle: roles of $[Ca^{2+}]_i$ and cross-bridge kinetics. J Physiol 1994;476(3):487–500.

[24] Matsumura K, Arai K, Zhong D, Saito F, Fukuta-Ohi H, Maekawa R, et al. Disruption of dystroglycan axis by ß-dystroglycan processing in cardiomyopathic hamster muscle. Neuromuscul Disord 2003;13:796–803.

[25] Kawada T, Nakatsuru Y, Sakamoto A, Koizumi T, Shin WS, Okai-Matsuo Y, et al. Strain- and age-dependent loss of sarcoglycan complex in cardiomyopathic hamster hearts and its re-expression by d-sarcoglycan gene transfer in vivo. FEBS Lett 1999;458:405–8.

[26] Wiegand V, Stroh E, Henniges A, Lossnitzer K, Kreuzer H. Altered distribution of myosin isoenzymes in the cardiomyopathic Syrian hamster (BIO 8.262). Basic Res Cardiol 1983;78(6):665–70.

[27] Malhotra A, Karell M, Scheuer J. Multiple cardiac contractile protein abnormalities in myopathic Syrian hamsters (BIO 53: 58). J Mol Cell Cardiol 1985;17(2):95–107.

[28] Pagani ED, Julian FJ. Rabbit papillary muscle myosin isozymes and teh velocity of muscle shortening. Circ Res 1984;54:586–94.

[29] Cappelli V, Bottinelli R, Poggesi C, Moggio R, Reggiani C. Shortening velocity and myosin and myofibrillar ATPase activity related to myosin isoenzyme composition during postnatal development in rat myocardium. Circ Res 1989;65:446–57.

[30] Josephson RA, Spurgeon HA, Lakatta EG. The hyperthyroid heart. An analysis of systolic and diastolic properties in single rat ventricular myoyctes. Circ Res 1990;66:773–81.

[31] Yamashita H, Sugiura S, Serizawa T, Sugimoto T, Iizuka M, Katayama E, et al. Sliding velocity of isolated rabbit cardiac myosin correlates with isozyme distribution. Am J Physiol 1992;263:H464–H472.

[32] Yamashita H, Sugiura S, Sata M, Serizawa T, Iizuka M, Shimmen T, et al. Depressed sliding velocity of isolated cardiac myosin from cardiomyopathic hamsters: evidence for an alteration in mechanical interaction of actomyosin. Mol Cell Biochem 1993;119:79–88.

[33] VanBuren P, Harris DE, Alpert NR, Warshaw DM. Cardiac V_1 and V_3 myosins differ in their hydrolytic and mechanical activation in vitro. Circ Res 1995;77:439–44.

[34] Sugiura S, Kobayakawa N, Momomura S, Chaen S, Omata M, Sugi H. Different cardiac myosin isforms exhibit equal force-generating ability in vitro. Biochim Biophys Acta 1996;1273:73–6.

[35] de Tombe PP, Wannengurg T, Fan D, Little WC. Right ventricular contractile protein function in rats with left ventricular myocardial infarction. Am J Physiol 1996;271:H73–H79.

[36] Nigro V, Okazaki Y, Belsito A, Piluso G, Matsuda Y, Politano L, et al. Identification of the Syrian hamster cardiomyopathy gene. Hum Mol Genet 1997;6:601–7.

[37] Towbin JA, Bowels NE. The failing heart. Nature 2002;415:227–33.

[38] Granzier HL, Irving TC. Passive tension in cardiac muscle: contribution of collagen, titin, microtubules, and intermediate filaments. Biophys J 1995;68(3):1027–44.

[39] Shah SB, Su FC, Jordan K, Milner DJ, Friden J, Capetanaki Y, et al. Evidence for increased myofibrillar mobility in desmin-null mouse skeletal muscle. J Exp Biol 2002;205:321–5.

Arteriosclerosis, Thrombosis, and Vascular Biology

JOURNAL OF THE AMERICAN HEART ASSOCIATION

Endothelium-Derived Hydrogen Peroxide Accounts for the Enhancing Effect of an Angiotensin-Converting Enzyme Inhibitor on Endothelium-Derived Hyperpolarizing Factor–Mediated Responses in Mice

Takako Fujiki, Hiroaki Shimokawa, Keiko Morikawa, Hiroshi Kubota, Makoto Hatanaka, M.A. Hassan Talukder, Tetsuya Matoba, Akira Takeshita and Kenji Sunagawa

Arterioscler. Thromb. Vasc. Biol. 2005;25;766-771; originally published online Feb 10, 2005;
DOI: 10.1161/01.ATV.0000158498.19027.75
Arteriosclerosis, Thrombosis, and Vascular Biology is published by the American Heart Association. 7272 Greenville Avenue, Dallas, TX 72514
 Print ISSN: 1079-5642. Online ISSN: 1524-4636